Local Surface Potential of π-Conjugated Nanostructures by Kelvin Probe Force Microscopy: Effect of the Sampling Depth

ARTICLE *in* SMALL · MARCH 2011

Impact Factor: 8.37 · DOI: 10.1002/smll.201001770 · Source: PubMed

8 AUTHORS, INCLUDING:

Vincenzo Palermo
Italian National Research Council
130 PUBLICATIONS **2,576** CITATIONS
SEE PROFILE

Oliver Fenwick
Queen Mary, University of London
39 PUBLICATIONS **488** CITATIONS
SEE PROFILE

Mats Fahlman
Linköping University
174 PUBLICATIONS **5,678** CITATIONS
SEE PROFILE

Franco Cacialli
University College London
256 PUBLICATIONS **7,436** CITATIONS
SEE PROFILE

Local Surface Potential of π-Conjugated Nanostructures by Kelvin Probe Force Microscopy: Effect of the Sampling Depth

Andrea Liscio, Vincenzo Palermo, Oliver Fenwick, Slawomir Braun, Klaus Müllen, Mats Fahlman, Franco Cacialli,* and Paolo Samorì**

***K**elvin probe force microscopy (KPFM) is usually applied to map the local surface potential of nanostructured materials at surfaces and interfaces. KPFM is commonly defined as a 'surface technique', even if this assumption is not fully justified. However, a quantification of the surface sensitivity of this technique is crucial to explore electrical properties at the nanoscale. Here a versatile 3D model is presented which provides a quantitative explanation of KPFM results, taking into account the vertical structure of the sample. The model is tested on nanostructured films obtained from two relevant semiconducting systems for field-effect transistor and solar cell applications showing different interfacial properties, i.e., poly(3-hexylthiophene) (P3HT) and perylene-bis-dicarboximide (PDI). These findings are especially important since they enable quantitative determination of the local surface potential of conjugated nanostructures, and thereby pave the way towards optimization of the electronic properties of nanoscale architectures for organic electronic applications.*

1. Introduction

The accurate estimation of the surface potential (SP) of an object with precision on the nanoscale is of importance for many applications in materials science and nanotechnology.[1] Such estimations can be accomplished by means of Kelvin probe force microscopy (KPFM),[2] a noncontact and noninvasive technique which provides a map of the SP of the sample under study. The SP is caused by the difference in work functions (WFs) of the probe and the sample, and can be estimated with a spatial resolution of a few tens of nanometers and a voltage resolution below 10 mV.[3] Surface and subsurface charges (e.g., due to dopants in the case of semiconductors and dielectrics, or due to polar self-assembled monolayers)[4] significantly affect the work function (and therefore the potential) either directly or via polarization effects.[5]

Dr. A. Liscio, Dr. V. Palermo
Instituto per la Sintesi Organica e la Fotoreattività-Consiglio Nazionale delle Ricerche
Via Gobetti 101, I-40129 Bologna, Italy
E-mail: palermo@isof.cnr.it
Dr. O. Fenwick, Prof. F. Cacialli
Department of Physics and Astronomy (CMMP Group) and London Centre for Nanotechnology
University College London
Gower Street London WC1E 6BT, UK
Email: f.cacialli@ucl.ac.uk

DOI: 10.1002/smll.201001770

Dr. S. Braun, Prof. M. Fahlman
Department of Physics, Chemistry and Biology
Linköping University
581 83 Linköping, Sweden
Prof. K. Müllen
Max-Planck Institute for Polymer Research
Ackermannweg 10, 55124 Mainz, Germany
Prof. P. Samorì
Nanochemistry Laboratory, ISIS
Université de Strasbourg and CNRS (UMR 7006)
8 allée Gaspard Monge, 67000 Strasbourg, France
Email: samori@unistra.fr

NANO MICRO small

KPFM has been successfully employed to investigate a great variety of materials,[6] including inorganic[7] and organic thin films,[7,8] as well as proteins,[9] across multiple length scales, from the meso- to the nanoscale.

2. A 3D Model for Surface Potential Measurements by KPFM

The SP measured by KPFM includes both intrinsic and extrinsic contributions: the former are due to the electronic properties of the object under study, whereas the latter are the result of experimental artifacts brought about by the measurement itself. In particular the extrinsic term includes all the geometrical or electrical contributions, as the finite size of the scanning probe and the relatively long-range nature of the electrostatic interactions, which can easily extend to several hundreds of nanometers in nonmetallic samples. This leads to imprecise estimations of the measured surface potential.[10] In particular, when the nanostructure size is smaller than few hundreds of nanometers, the potential measured is an average of the SP of the nanostructure and of the surrounding substrate.

In a previous work we devised a semiquantitative 2D model to remove this averaging artifact and applied this to semiconducting nanostructures.[11] This model takes into account the interaction between the tip and the sample surface, and the finite lateral size of the nanostructure, neglecting the third dimension, i.e., the vertical structure of the sample. In this paper we present a more exhaustive procedure to obtain the 2D potential map by KPFM considering that the sample is a 3D object, as evinced by Russell[12] in the case of more general noncontact scanning-probe microscopy techniques, thus allowing a more precise estimation of the electric potential of nanostructured electroactive materials such as thin layers, nanocrystals, etc.

The measured surface potential (SP_{meas}) obtained from KPFM data is described as a convolution between the real potential (SP_0) of the system under study and the artifacts (i.e., the extrinsic term), described by the transfer function of the microscope (Γ). Jacobs et al.[10c] defined Γ as proportional to the derivative of the tip–surface capacitance $\partial C/\partial z$, where the tip oscillates on the Z-axis perpendicular to the metallic sample surface. This approach has been described by Colchero et al.[10b] in terms of electrostatic interaction energy (W) of the system, defined as $W = \frac{\varepsilon_0}{2}\int_V \left|\mathrm{E}(\vec{r})\right|^2 d\vec{r}$, where V is the volume with non-vanishing electrical field $\mathrm{E}(\vec{r})$.[13] Using this approach, we propose a generalised definition of Γ as being proportional to the square modulus of the electrical field inside the sample ($|\mathrm{E}|^2$which can then be tested on metallic and semiconducting surfaces.

In KPFM measurements of dielectrics, the electric field of the tip penetrates into the sample; therefore both the surface and the sub-surface regions of the sample underneath interact with the tip. By generalising the concepts and the physical/mathematical tools used in the 2D model, a 3D model is devised which takes into account the interacting volume of the sample. The KPFM measurement can be described as a convolution which transforms 3D quantities (all the SP values inside the sample at the position (x,y,z), i.e., SP_0) into 2D observables (the SP_{meas} image), expressed as

$$SP_{\mathrm{meas}}\left(r_{//}\right) = \int_{\mathrm{surface}} dr'_{//} \int_0^{\infty} \Gamma\left(r'_{//} - r_{//}, z'\right) \cdot SP_0\left(r'_{//}, z'\right) dz'$$

$$\Gamma\left(r'_{//} - r_{//}, z'\right) = \lim_{\Delta r'_{//}, \Delta z' \to 0} \frac{\left|\mathrm{E}\left(r'_{//} - r_{//}, z'\right)\right|^2}{W\left(\Delta r'_{//}, \Delta z'\right)} \quad (1)$$

where W is the tip–sample electrostatic interaction energy calculated for an infinitely small volume element and $\vec{r}_{//}$ is the position vector of the tip on the sample surface. Integration is performed over the entire sample and the position vector ($\vec{r}'$) is decomposed in parallel ($\vec{r}_{//}$), lying on the surface (XY-plane), and perpendicular (z') components, with the Z-axis positive inside the sample. Γ is the kernel of the convolution representing the 3D point spread function,[10e] reaching a maximum value on the sample surface under the tip position (Γ_{000}). We define the effective volume, i.e., the portion of the sample interacting with the tip, as the set of all points inside the sample for which $\Gamma \geq 0.05 \cdot \Gamma_{000}$. In the case of monocomponent and homogeneous materials, both the morphological and the electrical properties do not vary inside the sample (i.e., the 3D volume is defined in the semispace located by the positive Z-axis). In the simplest case, together with the discontinuity due to the sample surface, SP_0 does not vary inside the sample. In the case of band-bending at the surface or at the heterojunction interface, the charge density only varies along the Z-axis, while the X- and Y- components are not modified. In both cases, the sample charge density is decoupled in two terms: the parallel (//) and perpendicular ($\perp$) terms with respect to the sample surface; thus we propose to decouple the corresponding components of the transfer function given by their product: $\Gamma = \Gamma_{//} \cdot \Gamma_{\perp}$.

The situation appears to be quite different for metals, because in this case the electric field does not penetrate significantly into the sample, as indicated by a very short (a few Ångstroms) Debye length, in turn a result of the high concentration and mobility of free electrons in these materials. However, the factorisation presented above is still valid if one describes in this case $\Gamma_{\perp}$ with a Dirac delta centred on the surface.

Conversely, in nonhomogeneous samples (including isolated nanostructures or thin films adsorbed on a substrate), the SP signal is averaged over the effective volume. Thus, the estimation of Γ becomes crucial to extract the real SP of the object under study from the measured SP value containing the surrounding material potential. The need to achieve equalisation of the Fermi energy in a heterojunction (at equilibrium) leads to a a flow of electrons from the low WF materials to the high WF ones. The charge redistribution across the materials forming the hetereojunction may lead to charge being accumulated mainly on the electrodes (as is usual in OLEDs, with a mere band tilting across the semiconductors),[14] or both on the metallic electrodes and in the semiconductor, with concomitant band-bending in such regions (in agreement with Poisson's equation).[15] The different situations are schematically illustrated in **Figure 1**. Control over the band-bending is therefore fundamental to tailor the

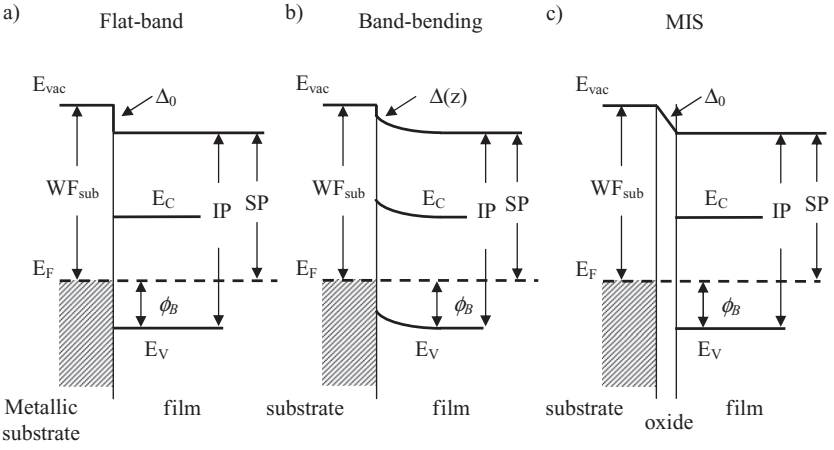

Figure 1. The energy-level alignment at a metal–organic semiconductor interface in a) a flat-band case, in b) a band-bending case, and in (c) a metal–insulator–semiconductor (MIS) heterojunction without band-bending (see main text for a detailed explanation).

interfaces between electrodes/dielectrics and organic semiconducting materials for micro- and nano-electronic devices.

The interpretation of experimental data and its correlation with the model mentioned above is carried out with the help of the band diagrams reported in Figure 1 for the case of a) a metal–semiconductor contact at flat-band, i.e., as occurring in the case of a metal work function close to a semiconductor work function, b) a metal–semiconductor heterojunction that reaches thermodynamical equilibrium via electron transfer from the semiconductor to the metal, with formation of a charge-space region (and subsequent band-bending) in the region of the semiconductor adjacent to the junction, and c) a heterojunction between a metal, an insulator, and a semiconductor, in which charge transfer occurs from the semiconductor to the metal, but no charge is stored in the insulator. The potential difference between the metal and the semiconductor film is thus dropped partially in the space-charge region in the semiconductor (with related band-bending) and partly on the insulator (with related band-tilting). For simplicity, we consider the sample SP referenced to the WF of the tip (i.e., $WF_{tip} = 0$).

As shown in Figure 1, the SP of a deposited organic semiconductor thin film can be written either as: a) the difference between the semiconductor ionization potential (IP) (i.e. the minimum energy needed to remove electrons from the sample) and the hole injection barrier (ϕ_B) at the film-substrate interface: $SP = IP - \phi_B$, where ϕ_B is defined as the difference between the Fermi energy (E_F) and the top of the valence states (E_V) of the deposited semiconductor, or b) as the sum of the substrate work function (WF_{sub}), defined as the difference between the vacuum level (E_{vac}) and E_F, plus ϕ_B, minus the energy shift at the interface (Δ_0): $SP = WF_{sub} + \phi_B - \Delta_0$.[15] For a better understanding, the energy of the conductive states (E_C) of the semiconductor film is shown in Figure 1.

In the case of metallic substrate, Δ_0 represents the WF difference between the substrate and the thin film plus a further shift due to the formation of new electronic states at the interface (i.e., interface dipoles). This picture considers both substrate and film as bulk materials (Figure 1a, flat-band case) and it is commonly used to describe the Au–P3HT heterojunction.[19] However, this picture can be generalised to describe the case of band-bending or when a thin oxide layer (i.e., a few nanometers thick) is formed on top of the substrate. In both cases, it is possible to generalise an energy shift Δ amounting to Δ_0 at the interface. In the case of band-bending (Figure 1b) where the charge density varies close to the interface causing an energy-level shift depending on the interface distance, Δ depends on the distance from the interface: $\Delta = \Delta(z)$, where $\Delta(0) = \Delta_0$. Increasing the complexity of the system, the third case is a Metal–Insulator–Semiconductor (MIS) heterojunction (Figure 1c), where the effect of the thin layer oxide is parameterised as a further component of the energy shift at the interface with the semiconductor film.

3. Comparative Surface Potential Measurements of P3HT and PDI

To test the proposed model we applied it to KPFM measurements of samples including: i) laterally uniform organic layers with different thicknesses (from a few tens to hundreds of nanometers), and known to feature negligible band-bending at the organic-substrate interface, and ii) nanostructures having both lateral and vertical nanometric dimensions, featuring significant band-bending. In particular, we chose two prototypical organic semiconductors, i.e., the p-type poly(3-hexylthiophenes) (P3HT),[11c,16] and the n-type perylenebis(dicarboximide) (PDI).[17] Both systems have been extensively employed for the fabrication of field-effect transistors and high-performance solar cells. The KPFM data obtained on these systems surface-processed into well-defined nanostructures were compared with ultraviolet photoemission spectroscopy (UPS) and macroscopic Kelvin Probe (KP) measurements.[18] The sampling depth in UPS is ca. 2 nm,[15] much smaller than the thickness of the deposited organic film, thus effective volume artifacts are neglected here. The KP technique is similar to KPFM, although the measurement is performed with a macroscopic oscillating probe with a diameter of several millimetres, and much larger probe-sample distances (d > 50 μm). The probe–sample system can therefore be described as a parallel-plate capacitor where the main portion of the volume of nonvanishing electric field is located between the tip and the sample. Considering the sample as a flat organic film of submicrometric thickness ($h << d$, where h is the film thickness and d is the probe–sample distance) and without the presence of any charge, the organic film gives a simple shift of the potential with respect to the values measured on clean substrates without thickness dependence.

As a test-bed we employed P3HT films deposited on two flat substrates featuring different electrical properties, i.e., evaporated Au (metal, WF = 5.1 eV) on mica and p-doped Si (resistivity 0.005 Ohm cm) exposing a thin native oxide

small NANO MICRO

layer (SiO_x, ca. 2 nm thick) with a mean-square roughness (R_{RMS}) of 0.4 ± 0.1 nm as measured on areas of ca. 1 μm^2 and 200 μm^2. Spin-coated P3HT (molecular weight $M_W \approx$ 50 kD) from a solution in $CHCl_3$ (concentration = 5 mg mL^{-1}) forms uniform layers with R_{RMS} of 3 ± 1 nm on both substrates. These uniform layers are composed of single nanofibril domains,[16d] randomly oriented and bundled together on a scale smaller than the KPFM lateral resolution. By varying the spinning rate during the deposition we modified the film thickness between a few nanometers to about 3 μm, as measured by profilometry.

Figure 2 reports the SP_{meas} values measured by KPFM (solid black squares) as a function of the film thickness, for a) Au and b) SiO_x–Si substrates. The ΔSP_{meas} values refer to the clean substrates, and the error bars correspond to the measured standard deviations. KPFM measurements revealed that the SP_{meas} in P3HT films supported on Au is independent of the film thickness, whereas the SP_{meas} determined on films supported on SiO_x was found, with increasing thickness, to decrease from about 4.45 eV down to an asymptotic value of ca. 4.23 eV. The KPFM results for P3HT films supported on Au agree with those obtained by KP measurements (open red circles, Figure 2a), with the two average values amounting to 4.44 ± 0.02 eV and 4.40 ± 0.01 eV, respectively. KPFM measurements of P3HT films supported on SiO_x showed an asymptotic behaviour, with a good agreement with both KP (open red circles, Figure 2b) and UPS data (open blue squares, Figure 2b) only for large film thicknesses (>100 nm). P3HT on SiO_x did not show measurable band-bending effects: KP, UPS, and KPFM measurements gave an SP of 4.27 ± 0.02 eV, 4.25 ± 0.05 eV, and 4.23 ± 0.01 eV for film thicknesses exceeding 100 nm, in agreement with values reported in literature.[19] Conversely, for smaller layer thicknesses (<100 nm) the SP measured with KPFM showed significant variations with respect to KP and UPS data, demonstrating the presence of an artifact due to the KPFM technique sampling depth.

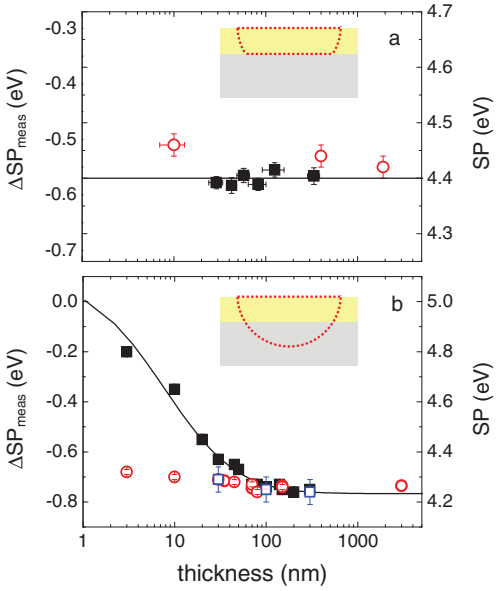

Figure 2. Film-thickness dependence of the SP_{meas} of P3HT film deposited on a) Au and b) SiO_x measured by KPFM (solid black squares), KP (open red circles), and UPS (open blue squares) techniques. The KPFM trend is fitted using the proposed model (line). For clarity, both the ΔSP (relative to the substrate) and the absolute SP (obtained using tips with known, calibrated WFs) are reported in the Y-axes. In the insets, schematic cartoons are shown of the effective volume extending into the organic layer on the substrate.

The weak interactions between the P3HT adsorbed film and the Au[19] and SiO_x[11c] substrates allows us to ascribe the contribution of the interface modification to the energetics of the P3HT–substrate interface as an energy shift as shown in Figure 1a, by considering that the overall SP results in being a simple sum of the contributions due to the deposited film and the substrate. Artifacts due to the lateral variations in SP can be easily excluded since amorphous P3HT films are homogeneous on a lateral scale of hundreds of nanometers: $SP_{meas}(r_{//}) = SP_{meas}$. In fact the measured potential does not depend on the measuring position, and Equation 1 is reduced to a 1D convolution depending on the film thickness (h), where the contributions of P3HT and the substrate can be separated:

$$SP_{meas}(h) = \int_0^h \Gamma_\perp \cdot SP_{P3HT}\, dz' + \int_h^\infty \Gamma_\perp \cdot SP_{substrate}\, dz' \qquad (2)$$

On a Au substrate, the KPFM measurement samples only the deposited film, since the second term of the equation is independent of h because $\Gamma_\perp$ is reduced to a Dirac delta. In KP and UPS measurements, SP_{P3HT} does not depend on the film thickness and Equation 2 can be written in the simpler form: $SP_{meas}(h) - SP_{substrate} = SP_{P3HT}$.

Conversely, the second term of Equation 2 plays an important role for thin P3HT films supported on SiO_x. To interpret results from this set of samples we neglect i) the Si band-bending (which is insignificant because of the high doping level of the substrate, concentration >10^{19} cm^{-3}), and ii) the local variation of the surface charge density due to the tip.[20] Within the limits of such approximations, the substrate behaves as a metal and its potential (i.e., $SP_{substrate}$) is assumed to match the WF of silicon, corrected by the potential shift due to the thin oxide layer (Figure 1c), which, having a constant value Δ_0, can be extracted from the integral. Hence, Equation 2 reduces to $SP_{meas}(h) = \alpha_h \cdot SP_{P3HT} + (1 - \alpha_h) \cdot SP_{substrate}$, where α_h is the Γ integral depending on the film thickness.

With increasing film thickness the contribution of the substrate decreases, up to a thickness of ca. 100 nm where the contribution of the substrate to the SP_{meas} vanishes and only P3HT contributes to the measured potential: $\lim_{h\to\infty} SP_{meas}(h) - SP_{substrate} = SP_{P3HT}$. Defining the asymptotic SP difference between the bulk value of P3HT and the clean substrate: $\Delta SP = SP_{P3HT} - SP_{substrate}$, Equation 2 becomes:

$$SP_{meas}(h) - SP_{substrate} = \Delta SP_{meas}(h) = \alpha_h \cdot \Delta SP \qquad (3)$$

where $0 < \alpha_h < 1$ contains all the details of the tip–sample system such as the electrical permittivities of the substrate[21] and the P3HT,[22] amounting to $\varepsilon_{Si} = 12$ and $\varepsilon_{P3HT} = 3$, respectively. This equation includes both the shape of the tip as well its distance from the surface. In general an analytical solution to

this equation is not trivial. The α_h function is calculated using a modified parallel-capacitor description, demonstrated in a previous work,[11b] in which the field is parameterised as $E \propto d_{eff}^{-\beta}$, with d_{eff} being the effective tip–sample distance and β the electrostatic force dependence. Upon modelling the tip–sample electrical field with finite element analysis, in which all the geometrical information has been obtained by the specifics of the tip's manufacturing company (ATEC-EFM-20 tip, Nanosensors), we estimate both parameters: $d_{eff} = 70$ nm and $\beta = 1.5$.

Thus, ΔSP is the only free parameter estimated from the measurements. The obtained fit curve (line in Figure 2b) agrees with the measured trend where the estimated SP_{P3HT}, amounting to 4.23 ± 0.02 eV, is close to the values measured with KP and UPS techniques, which do not show a significant SP-dependence on the P3HT thickness. Thus, the application of the above-described model suggests that the SP of P3HT in thin layers corresponds to the bulk value, and that any difference observed at the nanoscale with KPFM measurements is due to the effective volume averaging.

While P3HT has been used to assess the validity of the proposed model, we can apply it to a more complex system, i.e., objects of a nanometer size both in lateral and vertical dimensions, and/or films with relevant band-bending at the organic–substrate interface. We thus studied perylenebis(dicarboximide) (PDI) nanocrystals,[11a] featuring a lateral size between 10^2 and 10^3 nm and a thickness of up to a few hundreds of nanometers, which on SiO_x can show a strong band-bending due to the bulk charge redistribution.[23] When drop-cast from a chloroform solution on highly oriented pyrolytic graphite (HOPG), the PDI aggregates into flat, well-defined needlelike structures with different thickness (**Figure 3**a,b). The PDI SP_{meas} was found to vary with the film thickness (black squares in Figure 3c). The effective area contribution cannot be neglected and the KPFM image is a 3D convolution, where Equation 1 can be written as:

$$SP_{meas}(r_{//}, h) = \int_{surface} dr'_{//} \cdot \left[(1 - \Gamma_{//}) \cdot SP_{HOPG}(r'_{//}) + \Gamma_{//} \int_0^h \Gamma_{\perp} \cdot SP_{PDI}(r'_{//}, z')\, dz' \right] \quad (4)$$

The 3D function $SP_{PDI}(r'_{//}, z')$ represents the potential present in the PDI structures, and its projection along the Z-axis is the band-bending profile at the interface with the substrate modified by Γ.

The KPFM lateral resolution, which as mentioned earlier is a few tens of nanometers,[11b] allows us to neglect the potential variation at the boundaries of the nanostructures, thus making it possible to separate the integral into parallel and perpendicular components and to solve Equation 4 in a simple way.

Figure 3c shows the thickness-dependence of the SP of PDI as measured (black squares), after removal of the artifact due to effective-area lateral convolution ($\Gamma_{//}$-dependence, red triangles) and after removal of the effect of sampling depth (Γ-dependence, blue circles).

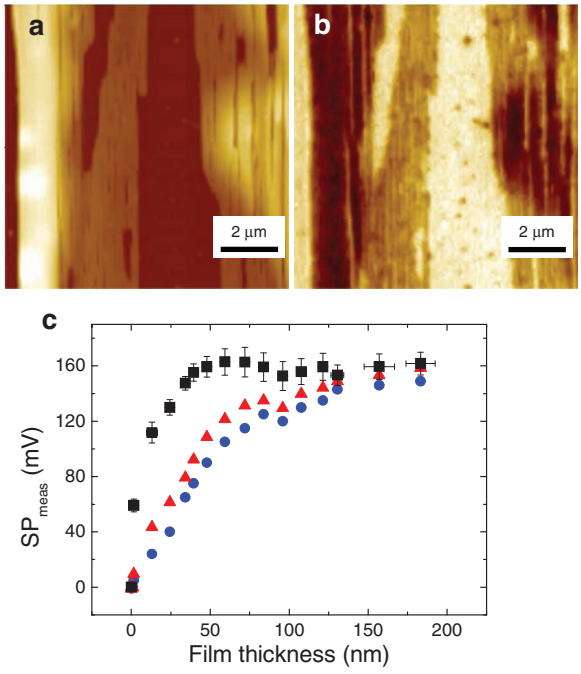

Figure 3. Atomic force microscopy topographic image (a) and corresponding KPFM image (b) of PDI structures on HOPG, where maximum (minimum) value is represented by white (black). c) The measured SP dependence on the film thickness (black squares). By removing the effective area artifacts (red triangles) and deconvoluting the sampling depth, the band-bending profile is obtained (blue circles). Z ranges = a) 120 nm, b) 190 mV.

Once the effective area artifacts are removed, the measured SP of PDI is a 1D function, which is shown in Figure 3c (red triangles). Here the h-dependence is given by the convolution between Γ and the band-bending profile $SP_{PDI}(z')$ where h represents the z' value sampled by the KPFM measurement, corresponding to the PDI film thickness. Thus, the $SP_{PDI}(z')$ trend (blue circles) is calculated by inverting Equation 4 using the deconvolution method reported in reference [24].

Upon removal of the effects due to the nanometric size of the sample (both in the Z-dimension and along the XY plane), we observe a dependence of the SP on the material's thickness, which is a direct visualization of the presence of band-bending at the organic–substrate interface.

4. Conclusion

In conclusion, to improve the understanding of the electronic properties of π-conjugated materials as active components for organic electronic applications, we have performed a comparative study on the estimation of the SP by KPFM, macroscopic KP and UPS. We have shown that the common belief of KPFM being a purely surface-sensitive technique is valid only for highly conductive (i.e., metallic) systems. Instead, for thin organic layers both the deposited and substrate materials contribute to the measured surface potential.

We devised a 3D model to single out the two contributions, showing that on P3HT films the sampling depth amounts to ca. 100 nm. The model was also applied to quantify the electronic properties of more complex nanostructured materials such as PDI needles on HOPG, where the organic nanostructure shows band-bending at the interface. By varying the film thickness, the real variations of SP due to, e.g., band-bending, can be determined from experimental artifacts. Our findings represent a step forward towards both the optimization of the properties of semiconducting nanostructured materials and the tuning of their interfaces with metal electrodes and dielectrics, being key steps in the fabrication of high performance (nano)electronic devices.

Supporting Information

Supporting Information is available from the Wiley Online Library or from the author.

Acknowledgements

This work was supported by the EC FP7 ONE-P large-scale project no. 212311, the Marie Curie projects ITN-SUPERIOR (PITN-GA-2009–238177) and THREADMILL (MRTN-CT-2006–036040), the NanoSci-E+ project SENSORS, the Regione Emilia-Romagna PRIITT Prominer Net-Lab and the International Center for Frontier Research in Chemistry (FRC).

[1] a) H. Ishii, K. Sugiyama, E. Ito, K. Seki, *Adv. Mater.* **1999**, *11*, 605; b) H. Ishii, N. Hayashi, E. Ito, Y. Washizu, K. Sugi, Y. Kimura, M. Niwano, Y. Ouchi, K. Seki, *Phys. Stat. Sol. A* **2004**, *201*, 1075; c) N. Koch, *ChemPhysChem* **2007**, *8*, 1438.

[2] a) M. Fujihira, *Annu. Rev. Mater. Sci.* **1999**, *29*, 353; b) M. Nonnenmacher, M. P. Oboyle, H. K. Wickramasinghe, *Appl. Phys. Lett.* **1991**, *58*, 2921.

[3] a) V. Palermo, M. Palma, P. Samorì, *Adv. Mater.* **2006**, *18*, 145; b) A. Liscio, V. Palermo, P. Samorì, *Acc. Chem. Res.* **2010**, *43*, 541.

[4] G. Latini, M. Wykes, S. Howorka, R. Schlapak, F. Cacialli, *Appl. Phys. Lett.* **2008**, *92*, 013511

[5] S. V. Kalinin, D. A. Bonnell, *Phys. Rev. B* **2001**, *63*, 125411.

[6] V. Palermo, A. Liscio, M. Palma, M. Surin, R. Lazzaroni, P. Samorì, *Chem. Commun.* **2007**, 3326.

[7] T. Meoded, R. Shikler, N. Fried, Y. Rosenwaks, *Appl. Phys. Lett.* **1999**, *75*, 2435.

[8] J. Lu, L. Eng, R. Bennewitz, E. Meyer, H. J. Guntherodt, E. Delamarche, L. Scandella, *Surf. Interf. Anal.* **1999**, *27*, 368.

[9] a) A. Gil, P. J. de Pablo, J. Colchero, J. Gomez-Herrero, A. M. Baro, *Nanotechnology* **2002**, *13*, 309; b) K. J. Kwak, S. Yoda, M. Fujihira, *Appl. Surf. Sci.* **2003**, *210*, 73.

[10] a) D. S. H. Charrier, M. Kemerink, B. E. Smalbrugge, T. de Vries, R. A. J. Janssen, *ACS Nano* **2008**, *2*, 622; b) J. Colchero, A. Gil, A. M. Baro, *Phys. Rev. B* **2001**, *64*, 245403; c) H. O. Jacobs, P. Leuchtmann, O. J. Homan, A. Stemmer, *J. Appl. Phys.* **1998**, *84*, 1168; d) S. V. Kalinin, S. Jesse, B. J. Rodriguez, J. Shin, A. P. Baddorf, H. N. Lee, A. Borisevich, S. J. Pennycook, *Nanotechnology* **2006**, *17*, 3400; e) E. Strassburg, A. Boag, Y. Rosenwaks, *Rev. Sci. Instrum.* **2005**, *76*, 083705; f) U. Zerweck, C. Loppacher, T. Otto, S. Grafstrom, L. M. Eng, *Nanotechnology* **2007**, *18*, 084006.

[11] a) A. Liscio, V. Palermo, D. Gentilini, F. Nolde, K. Müllen, P. Samorì, *Adv. Funct. Mater.* **2006**, *16*, 1407; b) A. Liscio, V. Palermo, K. Müllen, P. Samorì, *J. Phys. Chem. C* **2008**, *112*, 17368; c) A. Liscio, V. Palermo, P. Samorì, *Adv. Funct. Mater.* **2008**, *18*, 907.

[12] E. V. Russell, N. E. Israeloff, L. E. Walther, H. A. Gomariz, *Phys. Rev. Lett.* **1998**, *81*, 1461.

[13] J. D. Jackson, *Classical Electrodynamics*, 3rd ed., John Wiley & Sons, Inc., **1999**.

[14] T. M. Brown, F. Cacialli, *J. Polym. Sci., Part B: Polym. Phys.* **2003**, *41*, 2649.

[15] H. Lüth, *Surfaces and Interfaces of Solid Materials*, 3rd ed., Springer-Verlag, Berlin **1998**.

[16] a) H. Sirringhaus, P. J. Brown, R. H. Friend, M. M. Nielsen, K. Bechgaard, B. M. W. Langeveld-Voss, A. J. H. Spiering, R. A. J. Janssen, E. W. Meijer, P. Herwig, D. M. de Leeuw, *Nature* **1999**, *401*, 685; b) E. Mena-Osteritz, A. Meyer, B. M. W. Langeveld-Voss, R. A. J. Janssen, E. W. Meijer, P. Bäuerle, *Angew. Chem. Int. Ed.* **2000**, *39*, 2680; c) R. J. Kline, M. D. McGehee, E. N. Kadnikova, J. S. Liu, J. M. J. Frechet, *Adv. Mater.* **2003**, *15*, 1519; d) A. Zen, J. Pflaum, S. Hirschmann, W. Zhuang, F. Jaiser, U. Asawapirom, J. P. Rabe, U. Scherf, D. Neher, *Adv. Funct. Mater.* **2004**, *14*, 757; e) M. Surin, P. Leclère, R. Lazzaroni, J. D. Yuen, G. Wang, D. Moses, A. J. Heeger, S. Cho, K. Lee, *J. Appl. Phys.* **2006**, *100*, 033712.

[17] a) M. Cotlet, S. Masuo, G. B. Luo, J. Hofkens, M. Van Der Auweraer, J. Verhoeven, K. Müllen, X. L. S. Xie, F. De Schryver, *Proc. Natl. Acad. Sci. USA* **2004**, *101*, 14343; b) B. A. Jones, M. J. Ahrens, M. H. Yoon, A. Facchetti, T. J. Marks, M. R. Wasielewski, *Angew. Chem. Int. Ed.* **2004**, *43*, 6363; c) C. R. Newman, C. D. Frisbie, D. A. da Silva, J. L. Brédas, P. C. Ewbank, K. R. Mann, *Chem. Mater.* **2004**, *16*, 4436; d) F. Würthner, *Chem. Commun.* **2004**, 1564; e) V. Palermo, A. Liscio, D. Gentilini, F. Nolde, K. Müllen, P. Samorì, *Small* **2006**, *3*, 161; f) R. Dabirian, V. Palermo, A. Liscio, E. Schwartz, M. B. J. Otten, C. E. Finlayson, E. Treossi, R. H. Friend, G. Calestani, K. Müllen, R. J. M. Nolte, A. E. Rowan, P. Samorì, *J. Am. Chem. Soc.* **2009**, *131*, 7055; g) V. Palermo, E. Schwartz, C. E. Finlayson, A. Liscio, M. B. J. Otten, S. Trapani, K. Müllen, D. Beljonne, R. H. Friend, R. J. M. Nolte, A. E. Rowan, P. Samorì, *Adv. Mater.* **2010**, *22*, E81.

[18] J. S. Kim, B. Lägel, E. Moons, N. Johansson, I. Baikie, W. R. Salaneck, R. H. Friend, F. Cacialli, *Synth. Met.* **2000**, *111*, 311.

[19] J. E. Lyon, A. J. Cascio, M. M. Beerbom, R. Schlaf, Y. Zhu, S. A. Jenekhe, *Appl. Phys. Lett.* **2006**, *88*, 222109.

[20] Y. Rosenwaks, R. Shikler, T. Glatzel, S. Sadewasser, *Phys. Rev. B* **2004**, *70*, 085320.

[21] S. M. Sze, *Physics of Semiconductor Devices*, 2nd ed., Wiley-Interscience, New York **1981**.

[22] T. Li, P. P. Ruden, I. H. Campbell, D. L. Smith, *J. Appl. Phys.* **2003**, *93*, 4017.

[23] R. Schlaf, P. G. Schroeder, M. W. Nelson, B. A. Parkinson, P. A. Lee, K. W. Nebesny, N. R. Armstrong, *J. Appl. Phys.* **1999**, *86*, 1499.

[24] A. F. Carley, R. W. Joyner, *J. Electron. Spectrosc. Relat. Phenom.* **1979**, *16*, 1.

Received: October 7, 2010
Published online: January 31, 2011